DOI: 10.1002/chem.201000501

Atomistic Characterisation of Li^+ Mobility and Conductivity in $Li_{7-x}PS_{6-x}I_x$ Argyrodites from Molecular Dynamics Simulations, Solid-State NMR, and Impedance Spectroscopy

Oliver Pecher,[a] Shiao-Tong Kong,[b] Thorsten Goebel,[a] Vera Nickel,[b] Katja Weichert,[c] Christof Reiner,[b] Hans-Jörg Deiseroth,*[b] Joachim Maier,*[c] Frank Haarmann,*[d] and Dirk Zahn*[e]

Dedicated to Professor Bernd Harbrecht on the occasion of his 60th birthday

Abstract: The atomistic mechanisms of Li^+ ion mobility/conductivity in $Li_{7-x}PS_{6-x}I_x$ argyrodites are explored from both experimental and theoretical viewpoints. Ionic conductivity in the title compound is associated with a solid–solid phase transition, which was characterised by low-temperature differential scanning calorimetry, ^7Li and ^{127}I NMR investigations, impedance measurements and molecular dynamics simulations. The NMR signals of both isotopes are dominated by anisotropic interactions at low temperatures. A significant narrowing of the NMR signal indicates a motional averaging of the anisotropic interactions above 177 ± 2 K. The activation energy to ionic conductivity was assessed from both impedance spectroscopy and molecular dynamics simulations. The latter revealed that a series of interstitial sites become accessible to the Li^+ ions, whilst the remaining ions stay at their respective sites in the argyrodite lattice. The interstitial positions each correspond to the centres of tetrahedra of S/I atoms, and differ only in terms of their common corners, edges, or faces with adjacent PS_4 tetrahedra. From connectivity analyses and free-energy rankings, a specific tetrahedron is identified as the key restriction to ionic conductivity, and is clearly differentiated from local mobility, which follows a different mechanism with much lower activation energy. Interpolation of the lattice parameters as derived from X-ray diffraction experiments indicates a homogeneity range for $Li_{7-x}PS_{6-x}I_x$ with $0.97\le x\le1.00$. Within this range, molecular dynamics simulations predict Li^+ conductivity at ambient conditions to vary considerably.

Keywords: argyrodites · ionic mobility · lithium · molecular dynamics · NMR spectroscopy

Introduction

The peculiar structure of argyrodites is widely assumed to account for their high ionic conductivity.[1–4] This is well established for Ag- and Cu-argyrodites, but the recently discovered Li-argyrodites also exhibit high ionic mobility.[5] The latter class of compounds, that is, Li_7PS_6 and Li_6PS_5X (X = Cl, Br, I) is of particular interest for application in lithium ion batteries.

[a] Dipl.-Chem. O. Pecher, Dipl.-Chem. T. Goebel
Max-Planck-Institut für Chemische Physik fester Stoffe
Nöthnitzer Str. 40, 01187 Dresden (Germany)

[b] S.-T. Kong, V. Nickel, Dr. C. Reiner, Prof. Dr. H.-J. Deiseroth
Anorganische Chemie, Universität Siegen
Adolf-Reichwein-Straße 2, 57068 Siegen (Germany)
Fax: (+49) 271-740-2555
E-mail: deiseroth@chemie.uni-siegen.de

[c] Dr. K. Weichert, Prof. Dr. J. Maier
Max-Planck-Institut für Festkörperforschung
Heisenbergstraße 1, 70569 Stuttgart (Germany)
Fax: (+49) 711-689-1722
E-mail: s.weiglein@fkf.mpg.de

[d] Prof. Dr. F. Haarmann
Institut für Anorganische Chemie, RWTH Aachen
Landoltweg 1, 52074 Aachen (Germany)
Fax: (+49) 241-80-92288
E-mail: frank.haarmann@ac.rwth-aachen.de

[e] Prof. Dr. D. Zahn
Lehrstuhl für Theoretische Chemie/Computer Chemie Centrum
Friedrich-Alexander Universität Erlangen-Nürnberg
Nägelsbachstraße 25, 91052 Erlangen (Germany)
Fax: (+49) 9131-852-6565
E-mail: dirk.zahn@chemie.uni-erlangen.de

The crystal structure of cubic HT-Li_7PS_6 (high-temperature Li_7PS_6) may be characterised topologically by a tetrahedral close packing formed by the S atoms.[6,7] 136 tetrahedral holes are present in the unit cell. Four belong to PS_4 tetrahedra, and the remaining 132 S_4 tetrahedra per unit cell are only about 21% occupied by off-centred Li^+ ions. In Li_6PS_5I, one of the three crystallographically independent S atoms is substituted by an I^- ion. The tetrahedral close packing gives rise to a variety of interstitial positions, all corresponding to tetrahedra which differ essentially in terms of common corners, edges, or faces with adjacent PS_4 tetrahedra. For better classification, some of us recently introduced a systematic nomenclature of the interstitial positions (Table 1).[6] Depending on the different accessibilities to the interstitial sites, the Li^+ ions may experience short-range motions within confined regions, or long-range translational motions at macroscopic length scales. Only the latter phenomenon allows ionic conductivity.

For a detailed characterisation of Li^+ mobility/conductivity in this complex framework, we shall make use of a combination of experimental and atomistic simulation approaches. Whereas the atomistic mechanisms of Li^+ ion conductivity are explored from molecular dynamics (MD) simulations, the theoretical models are confirmed from experimental evidence. For this purpose, solid-state NMR measurements offer direct insights into the short-range mobility of the Li^+ ions as a function of temperature. On the other hand, electrochemical impedance spectroscopy yields the conductivity data of the bulk material, as well as the activation energy of the Li^+ ion conduction.

Results

Sample characterisation: Two samples of Li_6PS_5I obtained from solid-state synthesis[5] were proved to be single-phase material throughout the X-ray powder diffraction investigations. The lattice parameters of both samples, $a=10.1440(2)$ and $a=10.1422(2)$ Å, are not in agreement within the threefold standard deviation, indicating the existence of a homogeneity range for Li_6PS_5I corresponding to the formulation $Li_{7-x}PS_{6-x}I_x$.

Indeed, the syntheses with reactant concentrations corresponding to $x=0.90$ and $x=1.20$ lead to multiphase samples, showing Li_2S and LiI as impurities. The lattice parameters of the $Li_{7-x}PS_{6-x}I_x$ major phase could be determined as 10.138(1) and 10.145(1) Å for nominal compositions corresponding to $x=0.90$ and for $x=1.20$, respectively. On the other hand, the lattice parameters from single-crystal X-ray diffraction experiments of HT-Li_7PS_6 (metastable under ambient conditions) and Li_6PS_5I are $a=9.932(1)$ and $a=10.145(2)$ Å, respectively.[5–7] The latter value is in excellent agreement with the results of X-ray powder diffraction for the two-phase sample with the smallest amount of Li. Thus, the Li-deficient batches lead to practically stoichiometric $Li_{7-x}PS_{6-x}I_x$ with $x=1.00$, whereas the Li-rich batch is interpreted as the lower limit of the homogeneity range. The latter is deduced as $x=0.97$ by means of linear interpolation of the lattice parameters from single-crystal X-ray diffraction experiments. For the present study, single-phase powder samples corresponding to an x value of 0.99 (DSC and NMR measurements), as well as $x\approx1$ (impedance spectroscopy), were used.

On the basis of differential scanning calorimetry (DSC) experiments, a solid–solid transition was observed at 177 ± 2 K (Figure 1). This is in good agreement with previously published results from X-ray and neutron diffraction experiments, describing the high-temperature (HTM) and low-temperature modifications (LTM) of $Li_{7-x}PS_{6-x}I_x$ with $x\approx1$.[5,6]

NMR spectroscopy: To obtain detailed atomistic insights into the mobility of the Li^+ ions, a combination of temperature-dependent NMR spectroscopic experiments, impedance measurements, and molecular dynamics simulations was applied. Recent ^{7}Li NMR experiments on $Li_{7-x}PS_{6-x}I_x$ with $x\approx1$ showed a two-step motional narrowing of the NMR signals.[5,8–10] This was interpreted as a rigid lattice below 170 K, and a non-restricted motional process above 250 K. In the range between $170\leq T\leq250$ K an intermediate motional process is assumed. Dipole–dipole coupling was identified as the dominant mechanism for the line broadening of the ^{7}Li NMR signals.

Our ^{7}Li NMR experiments agree in principle with this investigation, but additional evidence for quadrupole coupling was observed from satellite transitions below 175 K (Figure 2, top). This is in agreement with the monoclinic crystal structure model of the LTM, with six crystallographi-

Table 1. Systematic nomenclature of the interstitial positions derived from a crystal chemical analysis of the 136 tetrahedral holes formed by the S atoms in the unit cell of Li_7PS_6 in accordance with references [5,6].

Tetrahedron type	Wyckoff notation of tetrahedron centre (special: type 5a)	neighbourhood description
0	4*b* (P)	blocked by P atoms forming rigid PS_4 tetrahedra
1	16*e*	common faces with PS_4 tetrahedra
2	48*h*	common edges with PS_4 tetrahedra
3	4*d*	four common corners (no common edge) with PS_4 tetrahedra
4	16*e*	three common corners with PS_4 tetrahedra
5	48*h*	two common corners, two common faces with PS_4 tetrahedra
5a	24*g*	trigonal planar position located in the centre of the common face of two type 5 tetrahedra

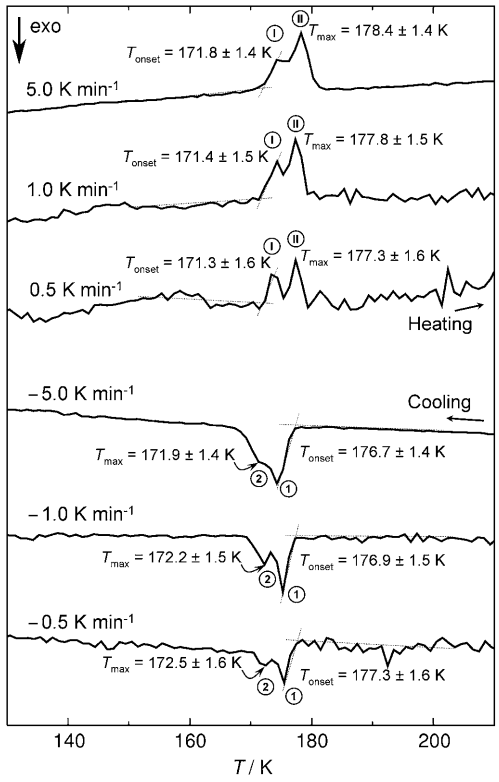

Figure 1. Dynamic scanning calorimetry measurements of $Li_{7-x}PS_{6-x}I_x$ with $x = 0.99$ performed at various cooling/heating rates. The two signals connected with the solid–solid phase transformation are labelled with Arabic numerals in the cooling curves and with Roman numerals in the heating curves, respectively. From extrapolation of the cooling/heating rates to 0 K min^{-1}, the critical temperature of the phase transformation is assessed as 177 ± 2 K.

cally independent Li positions of low symmetry.[6] The two-step motional averaging is therefore related to the phase transition from the HTM to the LTM, and an averaging of the dipole–dipole coupling above 175 K. Moreover, the transition temperature is in accordance with the DSC measurements.

A closer inspection of the crystal structure shows that I^- ions are located at positions of cubic symmetry, which are 12-fold coordinated by Li^+ ions. According to X-ray diffraction experiments each of these 12 Li^+ ions predominantly occupy one of three different sites (type 5a, 2 × type 5) resulting in I···Li distances of 3.59, 3.02, and 4.17 Å, respectively.[5] Thus, locally, a non-cubic environment of I^- can be expected. Due to the high nuclear quadrupole moment of −71.0 fm^2 of iodine,[11] ^{127}I NMR is very sensitive to deviations from cubic symmetry in the environment. For this reason, temperature-dependent ^{127}I NMR experiments appear particularly well suited to investigating the motional processes expected for the Li^+ ions. Motions of large amplitude are unattainable for the other atoms P, S, and I due to their atomic size.

The ^{127}I NMR wide-line experiments show a narrow signal at high temperature, which continuously broadens with decreasing temperature (Figure 2, bottom). The line shape can

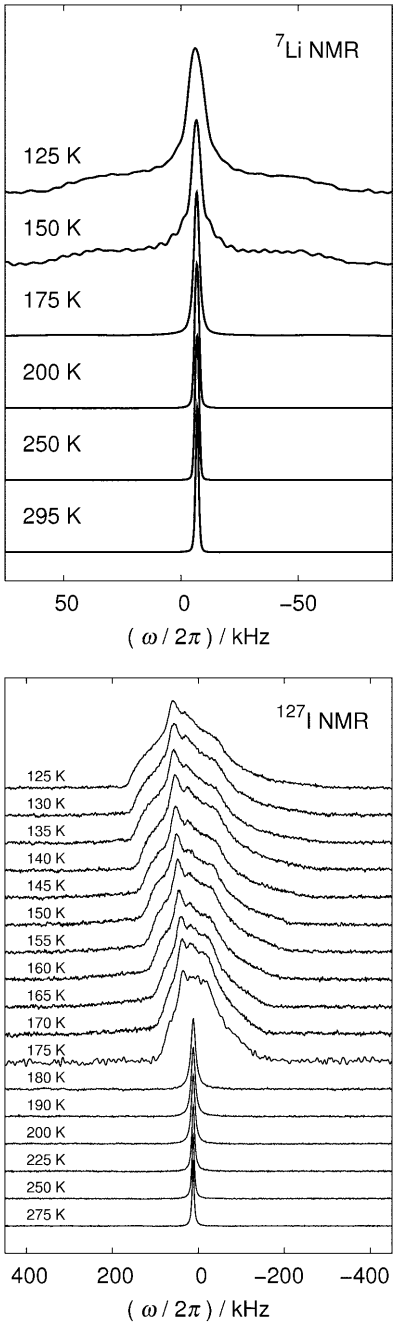

Figure 2. ^{7}Li (top) and ^{127}I NMR signals (bottom) of $Li_{7-x}PS_{6-x}I_x$ with $x = 0.99$ as a function of temperature.

be described by a Lorentzian between 525 and 180 K. An Arrhenius plot of the full width at half maximum (FWHM) indicates a thermally activated process with an activation energy of 0.040 eV (Figure 3). Such temperature-dependent broadening of the ^{127}I NMR signal can be related to various coupling mechanisms, for example, homo- and heteronuclear dipole–dipole coupling, second-order quadrupole coupling, anisotropic chemical shielding, and distributions of shifts. Anisotropic chemical shielding can be ruled out by the Lorentzian line shape of the NMR signal. According to calcula-

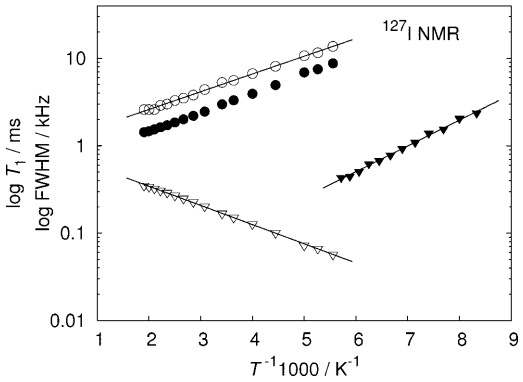

Figure 3. Arrhenius plots of FWHM and T_1 from ^{127}I NMR investigations. FWHMs from measurement (○) and estimates (●) based on the T_1 experiments, and T_1 values measured in the HTM (△) and LTM (▲) of $Li_{7-x}PS_{6-x}I_x$. The straight lines indicate the Arrhenius fits to the data.

tions of the second moments (M_2) using the van Vleck formula,[8,12] dipole–dipole coupling can be disregarded as the relevant mechanism of the line broadening (Table 2). The rigid lattice value of M_2 is far too small to explain the line

Table 2. Homo- and heteronuclear second moments (M_2): the calculations are based on the model of the crystal structure described in reference [5]. Li1a, Li1b, and Li2 represent the Li sites with distances to the coupling I^- ion of 4.17 (type 5), 3.02 (type 5), and 3.59 Å (type 5a), respectively. The contribution of ^{127}I–^{33}S coupling can be neglected due to the natural abundance of only 0.76% of ^{33}S. A Gaussian line shape has to be assumed to calculate of the full width at half maximum (FWHM = $\sqrt{8 \times \ln 2 \times M_2}$) because the corresponding expression is not defined for a Lorentzian.[13]

	M_2 [10^6 Hz^2]	FWHM [kHz]
^{127}I–^{31}P	0.007	0.20
^{127}I–^{7}Li1a	0.217	1.10
^{127}I–^{7}Li1b	1.229	2.61
^{127}I–^{7}Li2	0.466	1.61
^{7}Li2–^{7}Li2	1.445	2.83

width of the ^{127}I NMR signals at low temperatures in the HTM. Temperature-dependent MAS experiments removing the dipole–dipole coupling cause almost no reduction of the NMR signal width, in agreement with the results of the M_2 calculations (Figure 4, inset). Furthermore, they eliminate second-order quadrupole coupling as a relevant mechanism. The rotational sidebands of the MAS signals are a fingerprint of first-order quadrupole coupling and prove a violation of cubic symmetry for the local environment of the iodine positions (Figure 4). Measurements at lower magnetic field also show that a distribution of signal shifts is not the relevant mechanism of the line broadening (Figure 4, inset). These findings provide strong evidence that relaxation processes dominate the broadening of the ^{127}I NMR signals.

Since spin-lattice relaxation is very sensitive to motional processes,[8–10] temperature-dependent measurements of the spin-lattice relaxation times (T_1) were performed (Figure 3). The temperature-dependent behaviour of T_1 indicates a

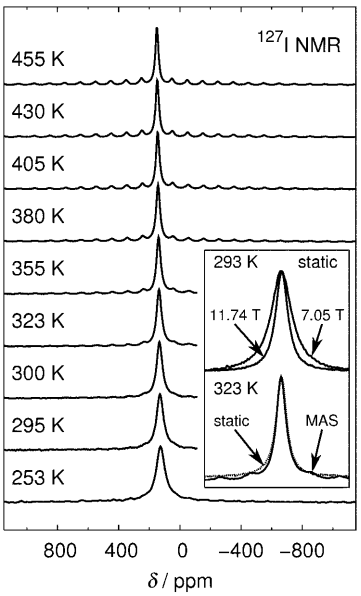

Figure 4. ^{127}I NMR MAS signals of $Li_{7-x}PS_{6-x}I_x$ with $x = 0.99$ as a function of temperature at 11.74 T. Inset: Comparison of static NMR signals in different magnetic fields at ambient temperature (top) and static and MAS NMR signals at 323 K (bottom). Both comparisons are presented on ppm scale to suppress the influence of the magnetic field on the shift interactions.

thermally activated motional process with an activation energy of 0.043 eV, in remarkable agreement with the activation energy determined from the FWHM of the signals (Figure 3). Both T_1 and the line width of the signals are hence most probably driven by the same motional process. To estimate the influence of T_1 on the signal width by lifetime broadening, FWHM $\approx 1/(2\,T_1)$ can be used (Figure 3).[13] The deviation of the FWHM obtained by this approximation and the temperature-dependent ^{127}I NMR experiments is probably due to spin–spin relaxation and/or details of the motional process. The increase of T_1 with temperature proves that the motion is fast in comparison with the timescale of the NMR experiments. The correlation time (τ_c), for example, the time between two jumps, is shorter than 10^{-8} s and decreases with increasing temperature in the HTM. The T_1 measured in magnetic fields of 11.74 and 7.05 T are equal within the experimental error. Thus, shift anisotropies can be ruled out as the origin of the spin-lattice relaxation.[10] Considering the small dipole–dipole couplings, quadrupole coupling has to be taken into account for the relaxation process.

Further ^{127}I NMR experiments show a sudden dramatic change of the line shape below 180 K (Figure 2, bottom). This is caused by quadrupole coupling, in agreement with the change of the crystal structure to lower symmetry as determined by neutron diffraction experiments.[6] The width of the signals increases with decreasing temperature (Figure 2, bottom). Lifetime broadening cannot account for this observation, as T_1 increases by an order of magnitude with the transition into the LTM (Figure 3). As a more reasonable explanation we suggest an influence of quadrupole coupling.

A more detailed analysis of the temperature dependence of the signal would call for ^{127}I NMR experiments in combination with line shape analysis. Temperature ranges in which the atomic motion is entirely frozen are especially suited for this purpose. The spectroscopic coupling parameters of NMR line shape analysis have to be compared with the results of quantum mechanical calculations to analyse the interactions. However, this is not within the scope of the present work, and will be the subject of future study.

The spin-lattice relaxation times increase with decreasing temperature (Figure 3). The activation energy of 0.059 eV for a thermally-activated motional process originates from the Arrhenius plot being larger than for the HTM. Strikingly, the activation energies for both phases are similar, hinting at similar motional processes. This issue will be discussed in more detail within the interpretation of the molecular dynamics results.

Impedance spectroscopy: Direct evidence of ionic conductivity and precise experimental conductivity values are obtained from impedance spectroscopy of polycrystalline $Li_{7-x}PS_{6-x}I_x$ with $x \approx 1$ (Figure 5). The capacity of the impedance signal of $\approx 10^{-11}$ F, corresponding to dielectric constants of about 50, clearly indicates bulk processes. Hence, grain boundary conductivity is of minor importance. At room temperature the conductivity was derived as 3.6×10^{-7} S cm^{-1}. In the measured temperature range between 298 and 248 K, the activation energy was found to be 0.32 eV (for the corresponding Arrhenius plot see Figure 5, inset). A detailed description of the conductivity measurements will be given elsewhere; here we emphasise the dominance of bulk conductivity for the polycrystalline sample. This is an important justification for the use of a relatively simple model for performing the molecular dynamics simulations, that is, a small super-cell mimicking a bulk single crystal. Though slight errors may be expected from fully ignoring interface effects, periodic boundaries, and the use of empirical force fields, the MD simulations should provide a reasonable agreement with the measured activation energy.

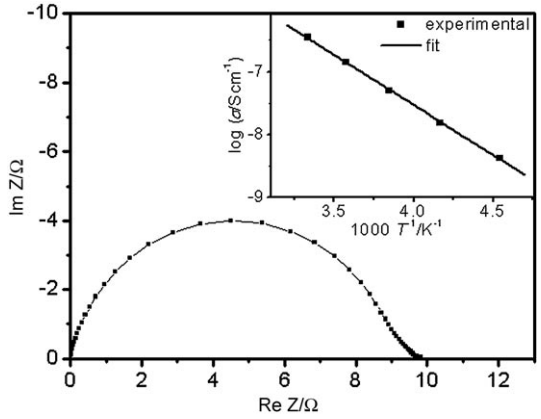

Figure 5. Nyquist diagram of the impedance spectrum of $Li_{7-x}PS_{6-x}I_x$ ($x \approx 1$) at ambient temperature, and the corresponding Arrhenius plot in the temperature range between 298 and 248 K (inset).

Molecular dynamics simulations: To explore the atomistic mechanisms of ionic mobility and conductivity in Li argyrodites, molecular dynamics simulations were employed for a series of $Li_{7-x}PS_{6-x}I_x$ single-crystal models. For $x = 0.00$, the model comprises of 256 S^{2-} ions located on Wyckoff position 4*a* ($F\bar{4}3m$). According to single-crystal investigations of the cubic HTM of $Li_{7-x}PS_{6-x}I_x$ with $x \approx 1$, a (randomly chosen) total of 16, 32, …, 256 of the above-mentioned S^{2-} ions are replaced by I^-, whilst removing the same number of Li^+ ions from the model, to mimic $x = 1/16, 2/16, \ldots, 1$. To cancel any bias concerning the initial distribution of Li^+ ions, all models were annealed at 1000 K before sampling the data. From the corresponding set of 17 independent simulation runs, ionic mobility/conductivity was explored for a hypothetical series of $Li_{7-x}PS_{6-x}I_x$ ($0 \le x \le 1$) single-crystal models. Each system was pre-equilibrated by energy minimisation runs to obtain ordered arrangements of the Li^+ ions according to relaxed structures. Ionic mobility was then explored from a series of 0.5 ns runs, during which the temperature was increased in steps of 25 K. Within the limited timescales accessible to molecular dynamics simulations, this procedure allows a qualitative pre-screening of ionic mobility as a function of temperature.[14] Li^+ mobility was found to occur as a two-step process. At low temperature the Li^+ ions fluctuate around the minimum energy configuration, which reflects a trigonal planar coordination by S^{2-} ions and the adjacent interstitial sites (type 5a and types 5, respectively). The latter are constituted by the centres of the two S_4/S_3I tetrahedra, the common face of which represents the trigonal coordination constellation. In the simulation runs performed at 250 K or below, the Li^+ ions were found to move over distances of up to 1.5 Å, yet remain confined to the two S_4/S_3I tetrahedra embedding the Li position at 0 K (here 1.5 Å refers to the maximum displacement observed in the course of thermal motion; crystal structure refinements indicated the displacement of the two type 5 sites as only 1.15 Å). Although this may be considered as local mobility, Li^+ conductivity requires larger displacements and hence the occupation of a variety of interstitial sites to allow ion migration throughout the unit cell.

The first evidence of such ionic displacements was observed in the molecular dynamics runs at 275 K. However, the overall conductivity is still too low to allow quantitative analyses on the basis of the short time sketches of 0.5 ns. On a qualitative basis, we can nevertheless state the existence of two stages of Li^+ movements, that is, local mobility at low temperature, and real conductivity over unrestricted length scales at high temperature. Generally, the quantitative analysis of ionic conductivity by molecular dynamics simulations is complicated by the limited timescales. On the basis of the few nanosecond runs accessible within reasonable computational demands, a considerable degree of heating is required to boost the number of Li^+ displacement events. We therefore performed additional long-term simulations of 1, 5 and

15 ns at temperatures of 750, 600 and 500 K, respectively. This allowed an Arrhenius plot to be made and the evaluation of Li^+ conductivity to be carried out within reasonable error margins (Figure 6). From this the activation energy

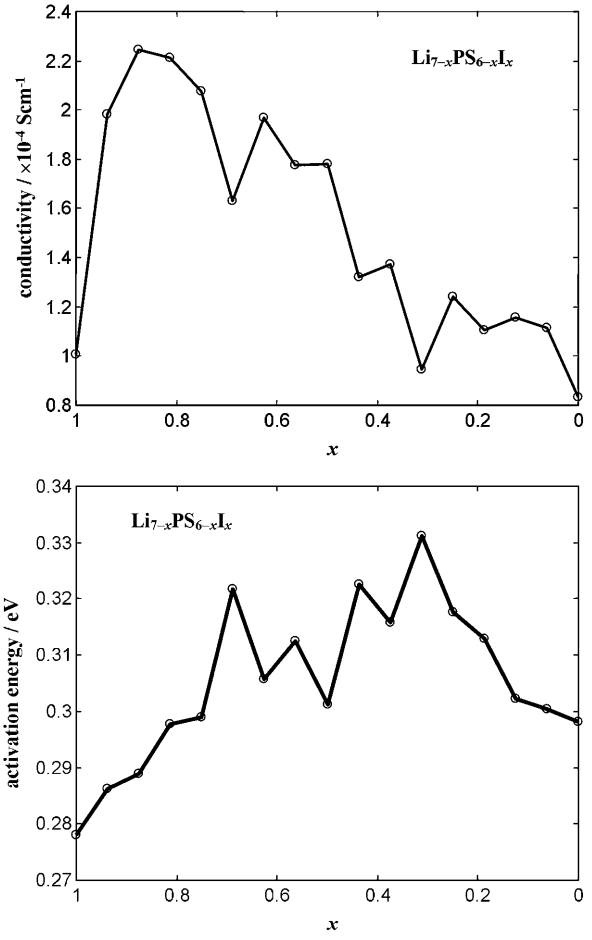

Figure 6. Top: Conductivity of $Li_{7-x}PS_{6-x}I_x$ single-crystal models ($4\times4\times4$ super-cells) calculated from 15 ns molecular dynamics simulation runs at 1 atm and 500 K. The best conductivity is observed for $Li_{7-x}PS_{6-x}I_x$ with $0.75\le x\le0.95$. Bottom: Activation barriers as derived from Arrhenius plots of the conductivity of $Li_{7-x}PS_{6-x}I_x$ modelled as solid solutions for the whole range $0\le x\le1$. The Arrhenius fits refer to conductivity data sampled from molecular dynamics simulations at 500 (15), 600 (5), and 750 K (1 ns), and are related to error margins of about 10%.

was estimated to be about 0.3 eV, which is in excellent agreement with the impedance spectroscopy measurements. The optimal conductivity is observed for $Li_{7-x}PS_{6-x}I_x$ with $0.75\le x\le0.95$. The Arrhenius plot allows extrapolation of the ionic conductivity to ambient temperature, which was assessed as about $3.0\times10^{-6}\,S\,cm^{-1}$ for $Li_{7-x}PS_{6-x}I_x$ with $0.75\le x\le0.95$. Although this hypothetical composition is, unfortunately, elusive to solid-state synthesis, our calculations nevertheless underline the importance of deviations from stoichiometric $Li_{7-x}PS_{6-x}I_x$ with $x=1.00$ in boosting Li^+ conductivity. Within the estimated homogeneity range of $0.97\le x\le1.00$, Li^+ conductivity at room temperature, as extrapolated from our molecular dynamics simulations, varies between 2.0–1.5 $\times10^{-6}\,S\,cm^{-1}$, respectively. As the activation energies are assessed at an accuracy of about 10%, the conductivity values extrapolated from 500 to 300 K should be considered only as rough estimates.

The close agreement of the activation energies to the Li conductivity as obtained from impedance measurements and molecular dynamics simulations provides strong support for our simulation models. The latter are particularly suitable for elaborating the atomistic mechanisms, which are indeed hard to assess from experimental information. A detailed characterisation of Li^+ conductivity may be based on an analysis of the occupation ratios of the different interstitial sites. From Boltzmann statistics we calculated the individual free energy levels of each interstitial type as denoted in Table 3. Apart from the difference in potential energy this also covers the increase in entropy, and, through extrapolation to lower temperature, also comparison to the experiments. The different interstitial sites are illustrated in Figure 7.

Table 3. Free enthalpies of Li sites in Li_6PS_5I and Li_7PS_6 as derived from 15 ns molecular dynamics runs at 500 K and 1 atm.

Tetrahedron type (Wyckoff position)	**Li_6PS_5I** free enthalpy [eV]	**Li_7PS_6** free enthalpy [eV]
type 5a (24*g*) and type 5 (48*h*)	0.0	0.0
type 4 (16*e*)	0.14	0.24
type 3 (4*d*)	0.39	0.22
type 2 (48*h*)	0.27	0.32
type 1 (16*e*)	unoccupied	unoccupied

Apart from the usual lattice vibrations, the fastest motional process of Li^+ dislocation is observed as local fluctuations around the type 5a positions. Indeed, the barrier to type 5a–type 5 fluctuations is too low to clearly discriminate individual sites from MD simulations at 500 K or above. However, the NMR experiments provide insights into such Li dislocation processes. Based on the relaxation times observed by NMR we suggest that the obtained signals arise from the type 5a–type 5 fluctuations. Thus, the activation energy of 0.040 eV determined by NMR experiments is assigned to this process. It is worth noting that these fluctuations only account for local mobility, and seem to persist in the LTM, as a similar activation energy is observed below 177 K. We conclude that the type 5a–type 5 fluctuations are active in both the LTM and the HTM, albeit within different local environments that account for the different shapes of the NMR signals, and only slightly different activation energies. Whereas this hypotheses is in contrast to the full ordering derived from neutron diffraction experiments at 170 K,[6] molecular dynamics simulations performed at 125 K indeed show type 5a–type 5 fluctuations, although at drastically reduced occurrence. We expect the envisaged low-temperature NMR experiments, combined with quantum calculation of the NMR coupling parameters, to shed more light on this issue.

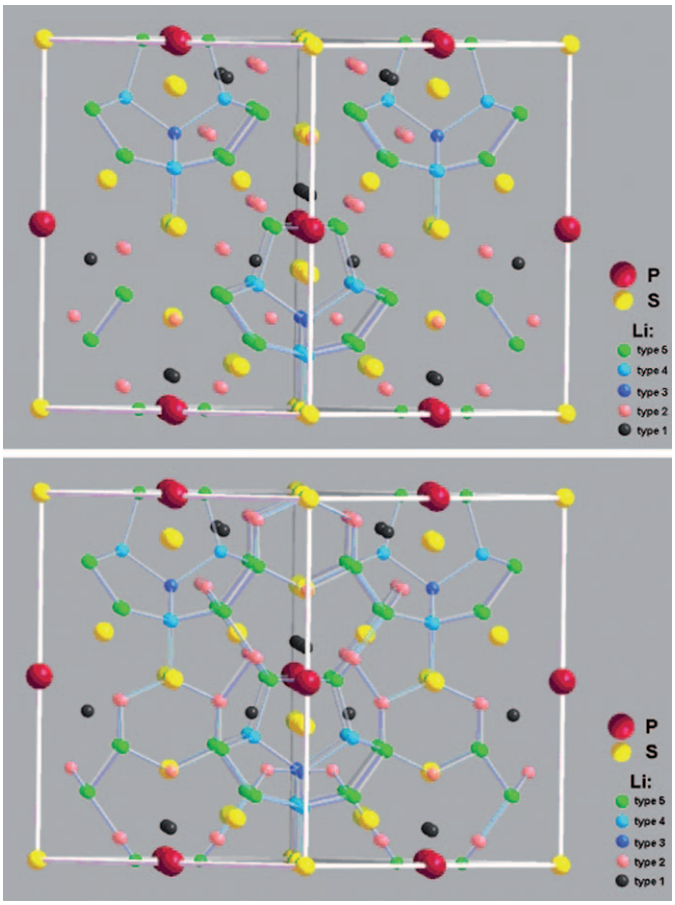

Figure 7. Illustration of the Li_7PS_6 unit cell including interstitial Li sites as denoted in Table 3. The most frequently observed constellation is represented by Li^+ ions fluctuating through the triangular coordination between the two adjacent type 5 tetrahedra (green). Ionic mobility is considered as Li^+ jumps between adjacent interstitial sites, that is, type 5, 4, 3, and 2 tetrahedra, whereas the type 1 tetrahedra remain unoccupied. Top: Connectivity map of adjacent interstitial Li sites (distance <2 Å) excluding the type 2 tetrahedra (pale red). In this picture, ionic mobility would be limited to short-range fluctuations within small regions. Bottom: Full conductivity throughout the whole crystal requires Li^+ migration through type 5, type 4, and type 2 interstitial sites. The latter reflect the restriction of the migration process and account for the activation barrier of ionic conductivity in Li_7PS_6 as well as Li_6PS_5I. The energetically unfavourable type 3 interstitials (dark blue) are connected in both pictures, despite not being of crucial relevance to ionic conductivity. Indeed, type 5–type 3–type 5 pathways may alternatively be replaced by type 5–type 4–type 5 pathways. The high-temperature molecular dynamics simulations indicate the latter route as the more active (refer also to Table 3).

In contrast to local mobility, Li^+ conductivity requires long-range ionic displacements. The latter may be interpreted in terms of subsequent jumps between adjacent S_4/S_3I tetrahedra, as illustrated for Li_6PS_5I by Figure 7, using a "connectivity map" in which nearby interstitial sites are connected by a line. Whereas all interstitial sites but type 2 are considered in Figure 7 (top), all putative interstitials are connected in Figure 7 (bottom). On the basis of the first connectivity map only short-range Li^+ movements are allowed. To provide full connectivity of the interstitial sites throughout the unit cell, it is imperative to also occupy positions of larger free energy level (0.27 eV). We hence suggest ionic conductivity to be confined by two barriers, of which the lower arises from the occupation of the Wyckoff position 16*e* (type 4) tetrahedra (0.14 eV), and the principal barrier is due to the Wyckoff position 48*h* (type 2) tetrahedra. Indeed, the latter energy level of 0.27 eV agrees well with the activation energies derived from the MD simulations, as well as the Arrhenius plots of the ionic conductivity obtained experimentally.

Conclusion

Li^+ ion mobility and conductivity in $Li_{7-x}PS_{6-x}I_x$ argyrodites have been explored from combined experimental and molecular dynamics simulation approaches. On the basis of DSC experiments and solid-state NMR spectroscopy, ionic conductivity in $Li_{7-x}PS_{6-x}I_x$ argyrodites has been found to occur through a solid–solid phase transition at 177 ± 2 K. Ionic mobility is observed even at low temperature, though below 177 K the displacement of Li^+ is confined to about 1.5 Å. This "local mobility" reflects fluctuations around the minimum energy configuration, which are given by trigonal planar coordinated sites (type 5a). For larger displacements the Li^+ ions must pass beyond the two S_3I tetrahedra, the common face of which constitutes the trigonal coordination. Hence, for Li^+ conductivity a series of interstitial sites must be reached. These sites are disfavoured by 0.14 and 0.27 eV, respectively. Both interstitial sites are essential to form a connective Li^+ pathway throughout the unit cell, and the configuration of higher energy accounts for the activation barrier to ionic conductivity.

Thus, the solid-state NMR measurements are closely connected to local mobility confined to about ±0.75 Å fluctuations around the trigonal planar coordinated sites, which is related to an activation barrier of only about 0.04 eV. This process is now suggested to occur in both phases, that is, above and below 177 K, although within different local environments. These change for the LTM→HTM transition, and provide an indirect signature of Li^+ conductivity in terms of a narrowing of the NMR line shape. On the other hand, the impedance spectroscopy measurements reveal conductivity directly, and along the same lines reveal the blocking to long-range Li^+ dislocation. Both experimental findings may be rationalised within a comprehensive picture of the atomistic mechanisms, as derived from MD simulations.

Experimental Section

Lattice parameters determination: X-ray diffraction was performed on two powder samples of nominal composition Li_6PS_5I from different batches using a Huber Gunier G670 diffractometer with $Cu_{K\alpha1}$ radiation ($\lambda=1.540598$ Å, internal standard LaB_6, $a=4.15692$ Å). The lattice parameters were determined using the WinCSD-2000 program package[15] with the same set of 28 reflections for both samples and 13 for LaB_6.

DSC measurements: Low-temperature differential scanning calorimetry (DSC) measurements were performed using a Netzsch DSC 204 heat-flux differential calorimeter equipped with a thermocouple E temperature sensor. The powdered sample (17 mg) was pressed into a pill in a glove box and transferred to an aluminium pan which was hermetically closed. A blank run with an empty aluminium pan was subtracted from the raw data. Temperature calibration was performed by a one-point calibration with n-hexane.

NMR spectroscopy: ^{7}Li and ^{127}I NMR spectroscopy investigations were carried out with a Bruker AVANCE and a Tecmag Apollo spectrometer, with magnetic fields of 11.74 and 7.05 T. The corresponding frequencies of ^{7}Li and ^{127}I at 11.74 T are 194.373 MHz and 100.071 MHz, respectively. The frequency corresponding to ^{127}I in the low magnetic field is 60.026 MHz. The ^{7}Li and ^{127}I NMR signals are referred to saturated solutions of LiCl and KI in D_2O, respectively. All experiments were performed on powder samples of randomly oriented crystallites. The sample was enclosed in a sealed glass ampoule for wide line experiments at 11.74 T. Magic angle spinning (MAS) experiments in both magnetic fields were carried out in 4.0 mm ZrO_2 rotors using Bruker double resonance probes. Wide line measurements at 7.05 T were also performed with this configuration.

^{7}Li NMR signals were recorded in a low-Q wide line probe (NMR-Service, Erfurt, Germany) over a temperature range of 295 to 125 K. The temperatures were adjusted with a flow of helium gas in a Janis research supertran-VP cryostat system (Janis Research Company, Wilmington, MA). Single pulse detection was employed for measurements above 150 K, and an echo sequence with pulses of equal duration of 2.2 μs for experiments at lower temperatures.

Wide-line variable-temperature ^{127}I NMR signals and spin-lattice relaxation times (T_1) were recorded between 525 and 125 K. The adjustment of the temperature was implemented by a flow of nitrogen gas. Down to a temperature of 180 K the wide line ^{127}I NMR signals were detected using a single pulse experiment with high-intensity pulses of 1.5 μs duration and a relaxation delay of 0.5 s. For temperatures below 180 K an echo sequence with pulses of equal duration of 1.0 μs and a relaxation delay of 1.0 s was applied. The interpulse time was optimised to 40 μs to avoid distortions of the line shape of the NMR signal. A saturation pulse sequence was applied in the T_1 measurements.

Temperature-dependent MAS experiments were carried out with a rotation frequency of 10 kHz. Single pulse experiments with hard pulses of 2.0 μs duration were applied. The adjustment of the temperature was achieved by a flow of nitrogen gas. To account for sample heating under MAS conditions the temperature was corrected considering the isotropic ^{207}Pb shift in solid $Pb(NO_3)_2$.[16] On this basis, a temperature offset of about 30 K was added to all measurements. ^{127}I NMR wide line, MAS, and T_1 measurements at 7.05 T were performed at ambient temperature.

Impedance spectroscopy: The electrochemical cell was: Li/$LiClO_4$ (1 M)/Li_6PS_5I/$LiClO_4$ (1 M)/Li. Both sides of the isostatically pressed Li_6PS_5I pellet ($p \approx 500$ MPa) were covered with porous polypropylene sheets (Cellguard2400). A drop of liquid electrolyte (1 M $LiClO_4$ in propylencarbonate) was added to this pellet, and then the lithium foil was attached. The custom-made measuring cell contains two stainless steel cylinders as terminal electrical contacts, each of them located in one part of a two-part screwable teflon container. The cell was assembled in a glove box ($O_2 \leq 0.1$ ppm, $H_2O \leq 0.3$ ppm) and the measurements were performed in a closed-cycle He refrigerator cryostat (Leybold RDK 10–320, compressor unit Leybold RW2, temperature controller Lakeshore 330). Impedance spectra were recorded with a High Frequency Dielectric Analyzer (Novocontrol) in the frequency range of 10^7–1 Hz. The temperature was varied between ambient temperature (298 K) and 248 K. The obtained spectra were evaluated using the Zview software package.

Molecular dynamics simulations: The simulation model comprised a 4×4×4 super-cell of Li_7PS_6/Li_6PS_5I, the interactions of which are described by a combination of Coulomb and Van der Waals potentials.[17] Both compounds may be described in terms of Li^+, S^{2-}, I^-, and $(PS_4)^{3-}$ moieties, which experience ionic binding. Within the $(PS_4)^{3-}$ tetrahedra, a large degree of covalent binding implies the use of partial charges, which were derived as +1.42 and −1.105 for P and S, respectively, using ab initio calculations at the MP2/6-311G** level. For the remaining Li, S and I ions, charges of +1, −2 and −1 are assumed, respectively. Throughout all simulations, the PS_4 tetrahedra were modelled as rigid moieties, the interatomic distances of which were adopted from crystallographic data.[5] To each super-cell configuration, periodic boundary conditions were applied, and Ewald summation with a real space cut-off of 10 Å was used. The molecular dynamics simulations were performed in the constant-temperature, constant-pressure (here: pressure set to 1 atm) ensemble.[18] For temperatures up to 1000 K, a simulation time-step of 2 fs was found to be appropriate.

Acknowledgements

D.Z. gratefully acknowledges the high-performance computing resources provided by the ZIH Dresden. We thank Dr. Stefan Hoffmann and Susann Scharsach for low-temperature DSC measurements and fruitful discussions. Furthermore, we thank Dr. Horst Borrmann and Steffen Hückmann for X-ray powder diffraction measurements.

[1] F. Boucher, M. Evain, R. Brec, *J. Solid State Chem.* **1993**, *107*, 332–346.
[2] M. Evain, E. Gaudin, F. Boucher, V. Petricek, F. Taulelle, *Acta Crystallogr. Sect. A* **1998**, *54*, 376–383.
[3] E. Gaudin, H. J. Deiseroth, T. Zaiß, *Z. Kristallogr.* **2001**, *216*, 39–44.
[4] T. Zaiß, H. J. Deiseroth, *Z. Kristallogr. New Cryst. Struct.* **2006**, *221*, 119–120.
[5] H. J. Deiseroth, S. T. Kong, H. Eckert, J. Vannahme, C. Reiner, T. Zaiß, M. Schlosser, *Angew. Chem.* **2008**, *120*, 767–770; *Angew. Chem. Int. Ed.* **2008**, *47*, 755–758.
[6] S. T. Kong, H. J. Deiseroth, C. Reiner, Ö. Gün, E. Neumann, C. Ritter, D. Zahn, *Chem. Eur. J.* **2010**, *16*, 2198–2206.
[7] S. T. Kong, Ö. Gün, B. Koch, H. J. Deiseroth, C. Reiner, H. Eckert, *Chem. Eur. J.* **2010**, *16*, 5138–5147.
[8] A. Abragam, *Principles of Nuclear Magnetism*, Oxford University, Oxford, **1961**.
[9] C. P. Slichter, *Principles of Magnetic Resonance*, 3rd ed., Springer, Berlin, **1990**.
[10] H. W. Spiess, *NMR, Basic Principles and Progress, Dynamic NMR Spectroscopy*, Springer, Berlin, **1978**.
[11] R. K. Harris, E. D. Becker, *J. Magn. Reson.* **2002**, *156*, 323–326.
[12] J. H. van Vleck, *Phys. Rev.* **1948**, *74*, 1168–1183.
[13] E. Fukushima, S. B. W. Roeder, *Experimental Pulse NMR: A Nuts and Bolds Approach*, Addison-Wesley Publishing Company, Oxford, **1981**.
[14] O. Hochrein, D. Zahn, *Solid State Ionics* **2009**, *180*, 116–119.
[15] L. G. Akselrud, P. Yu. Zavalii, Yu. Grin, V. K. Pecharski, B. Baumgartner, E. Wölfel, *Mater. Sci. Forum* **1993**, *133–136*, 335–340.
[16] A. Bielecki, D. P. Burum, *J. Magn. Reson. Ser. A* **1995**, *116*, 215–220.
[17] S. L. Mayo, B. D. Olafson, W. A. Goddard III, *J. Phys. Chem.* **1990**, *94*, 8897–8909.
[18] I. T. Todorov, W. Smith, *Phil. Trans. R. Soc. A* **2004**, *362*, 1835–1852.

Received: February 25, 2010
Published online: June 11, 2010

